Accidental bound states in the continuum in acoustic resonators with rotating obstacles

Yuhang Yin ,[1,2,3,*] Qilin Duan,[2,*] Shan Zhu,[1] Jing Li,[2] Zuoti Xie,[1,4,†] Cheng-Wei Qiu,[3] and Huanyang Chen [2,‡]

[1]*Quantum Science Center of Guangdong–Hong Kong–Macao Greater Bay Area (Guangdong), Shenzhen 518045, China*

[2]*Department of Physics, College of Physical Science and Technology and Pen-Tung Sah Institute of Micro-Nano Science and Technology, Xiamen University, Xiamen 361005, China*

[3]*Department of Electrical and Computer Engineering, National University of Singapore, Singapore 117583, Singapore*

[4]*Department of Materials Science and Engineering, MATEC, Guangdong Technion - Israel Institute of Technology, Shantou 515063, China*

(Received 21 May 2024; revised 20 July 2024; accepted 23 July 2024; published 5 August 2024)

Bound states in the continuum (BICs) are embedded states in the radiation spectrum, which have garnered significant interest across various areas, including photonics and acoustics. In this work, by introducing rotational obstacles into acoustic resonators, we report a series of accidental BICs in coupled waveguide-resonator systems. We demonstrate that a general type of accidental BICs would emerge at specific rotating angles, supported by the mode symmetries at the boundary interface between resonators and attached waveguides. We further demonstrate that the presence or absence of accidental BICs is closely related to the geometric parameters of resonators and obstacles, and can be predicted by the mode evolution within closed resonators. Additionally, we show that two BICs of an individual mode could converge, merge, and vanish in a single resonator by changing the geometry parameters. We also explore the topological origins of these phenomena. Our study provides an efficient way to manipulate and engineer BICs through rotating obstacles in acoustic resonator systems.

DOI: 10.1103/PhysRevB.110.054201

I. INTRODUCTION

In recent years, there has been a growing focus on high-Q resonances, driven by their significant potential applications in sensors and lasers [1–5]. Bound states in the continuum (BICs) have emerged as a viable pathway to achieve high-Q resonance [6,7]. The concept of BIC originated from the quantum system [8], and then extended into different physical systems like acoustic waves [9–19], water waves [17,20–23], optics, and photonics systems [24–29]. BICs are unique resonate states that exist within the energy spectrum of extended states but remain perfectly localized and do not radiate energy, thus are also known as trapped modes or embedded eigenmodes. Due to the nonradiative nature of BICs, these modes exhibit zero radiation loss, which theoretically results in an infinite quality (Q) factor. Based on the physical mechanism of the formation of BICs, they can be classified as symmetry-protected (SP) BICs [10,11,25,29,30], Friedrich-Wintgen (FW) BICs [28,31,32], Fabry-Perot (FP) BICs [24,33–35], and accidental BICs [26,35,36].

In acoustics, BICs, alternatively referred to as trapped modes, were first observed in the acoustic waveguide inserted with a parallel plate obstacle [9]. Furthermore, the acoustic waveguide system with different shapes and positions of the obstacles inside was also demonstrated to support quasitrapped mode [10–19]. Recently, acoustic resonators have gained popularity in investigating BICs, especially open coupled waveguide-resonator systems for the prevalence of achieving high-Q resonance with simple structures and easy fabrication [37–50]. For such integrated systems, the effective non-Hermitian Hamiltonian method can be applied to search for the zero point of the imaginary part of complex eigenfrequency, corresponding to the zero coupling between waveguides and resonators [7,51,52]. Some pioneering works have elucidated the existence of SP BICs [43,45,48], FW BICs [37–40,43,45,46], accidental BICs [40,45,48], and FP BICs [37,44,50] in coupled waveguide resonators. Most of the SP BICs are found in such systems with mirror symmetry C_{2v} [7], and FW BICs are supported by the destructive interference of two or more resonant modes within cavities. Accidental BICs arise from parameter tuning, such as the waveguide positions [45,48]. Meanwhile, acoustic BICs have found applications in sound emission enhancement [42], perfect absorption [49,50,53], and so on. In optics, the corporation of dielectric scatters into waveguides or cavities has been demonstrated to support accidental BICs or selective excitation of quasi-BICs (QBICs) without symmetry preserved [35,36,54]. However, this phenomenon remains underexplored in finite acoustic resonators, which possess diverse mode distributions that could enable innovative ways to manipulate BICs, such as merging BICs within a single resonator [35,44].

In this work, in the presence of rotating obstacles, we demonstrate the existence of accidental BICs in coupled waveguide-resonator systems. The rotation of obstacles breaks the symmetry of the resonators and relocates the eigenmode patterns, translating the BIC into QBIC. However, with the increase of rotation, the QBIC will translate into accidental BIC at a specific angle, where a symmetric mode distribution at the interface between the resonator and

*These authors contributed equally to this work.
†Contact author: zuoti.xie@gtiit.edu.cn
‡Contact author: kenyon@xmu.edu.cn

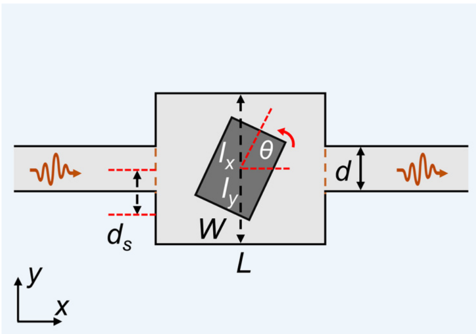

FIG. 1. Schematic of rotating obstacle in coupled-waveguide rectangular resonator system.

the coupled waveguide appears. The formation angles of the BICs can be tuned by the geometry parameters of the waveguides and obstacles, and we also calculate the eigenmodes in two-dimensional (2D) closed resonators to get the converging value of BIC angles. The emergence of accidental BICs is also linked to the geometry parameters of the systems, such as the obstacle size and the position of attached waveguide. This phenomenon can also be well predicted through the analysis of mode evolution within enclosed resonators. Furthermore, we also observe multiple accidental BICs in high-order resonant modes, demonstrating their converging, merging, and vanishing by simply altering the length of the resonator. Finally, we reveal the topological origins of the merging process. We systematically investigate the relationship of the Q factor with several asymmetry parameters and apply the coupled-mode theory (CMT) [43,52] to elucidate the transmission spectra of the QBICs. Our study provides a new paradigm for the manipulation of accidental BICs in acoustic resonators, which may find applications in acoustic sensors, filters, and so on.

II. ACCIDENTAL BICS IN 2D RECTANGULAR RESONATORS

To begin with, we investigate a coupled waveguide-resonator system depicted in Fig. 1. The dimensions of the rectangular resonator are $L = 90$ mm, $W = 80$ mm, embedded with a small rectangular obstacle with dimensions of $l_x = 30$ mm, $l_y = 45$ mm. The rotational angle is denoted by θ, and the width of the attached waveguides is set as $d = 30$ mm. According to the effective non-Hermitian Hamiltonian, the coupled system would have a complex eigenfrequency $\omega = \omega_0 - i\gamma$, where ω_0 and γ denote the resonant frequency and radiative decay rate, respectively. The Q factor of eigenmodes can be calculated by $Q = \omega_0/2\gamma$, and eigenmodes are denoted as M_{mn} depending on the number of the antinodes along the x and y axis. Here, commercial finite-element method (FEM) software COMSOL Multiphysics is utilized to acquire the eigenmodes and Q factors. The speed of sound and density of air are 343 m/s and 1.21 kg/m^3, respectively. Due to the symmetry of the system, we set the range of rotational angle θ between 0° to 90°. We first calculate the eigenfrequencies and Q factors within the rotational range and the excited transmission spectrum, as shown in Figs. 2(a) and 2(b).

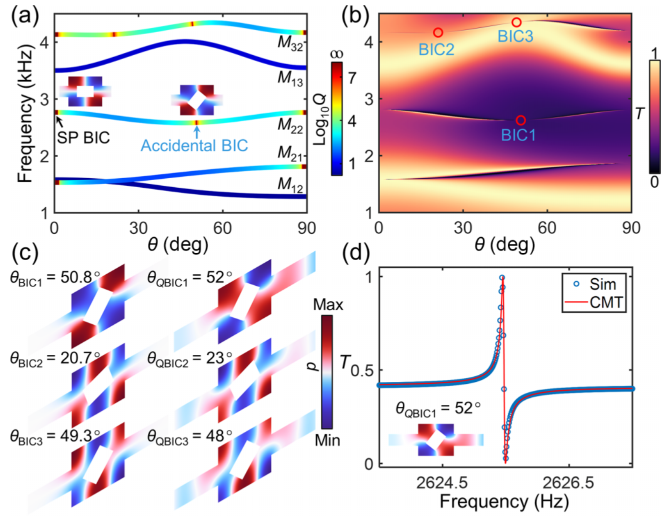

FIG. 2. Accidental BICs in 2D rectangular resonators. (a) Eigenmode spectra and Q factors. Insets show the patterns (total acoustic pressure) of BIC. (b) transmission spectra with respect to angle θ in a 2D rectangular resonator system. (c) Eigenmode patterns of the accidental BICs and QBICs within the calculated frequency range. (d) The transmission spectrum of QBIC with $\theta = 52^\circ$ using CMT and simulations. The inset shows a pattern of QBIC.

Here, we only consider the coupling of the first propagating mode of the waveguide, and the frequency range is set as 1000 to 4500 Hz, where five eigenmodes of the resonator, $M_{21}, M_{12}, M_{22}, M_{31}$, and M_{32}, are considered, respectively. Due to significant coupling effects with the waveguide, the resonance modes exhibit multiple nodal distributions in the propagation direction, while reserve one node number in the y direction, such as M_{21} and M_{31}, consistently displaying modes with low Q factors. Conversely, modes such as M_{12}, M_{22}, and M_{32}, which exhibit a dual nodal distribution perpendicular to the propagation direction, possess the capability to sustain high-Q modes.

Specifically, the structure reserves symmetries when $\theta = 0^\circ$ and 90° for these modes, which can be seen as regular resonators alternatively. Therefore, six SP BICs can be found as shown in Fig. 2(a), which have infinite Q factors. We can also find the vanishing line widths when approaching these BICs in the transmission spectrum shown in Fig. 2(b). When θ deviates from these two angles, M_{12}, M_{22}, and M_{32} would collapse into QBICs because of the symmetry breaking of the structure. However, when the rotation reaches the specific angles ($\theta_{\mathrm{BIC1}} = 50.8^\circ$, $\theta_{\mathrm{BIC2}} = 20.7^\circ$, and $\theta_{\mathrm{BIC3}} = 49.3^\circ$), modes M_{22} and M_{32} would translate into BICs again from QBICs, classified as accidental BIC1-3 here. This transformation is also characterized by the observation of approaching infinite Q factor and vanishing linewidth, as depicted in Figs. 2(a) and 2(b). The eigenmode patterns of the BICs and QBICs are provided in Fig. 2(c) and the rotation angles here are set as $\theta_{\mathrm{QBIC1}} = 52^\circ$, $\theta_{\mathrm{QBIC2}} = 23^\circ$, and $\theta_{\mathrm{QBIC3}} = 48^\circ$. Finally, we calculate the transmission spectrum of the QBIC1 shown in Fig. 2(d). Besides, the transmission spectra of the QBIC2 and QBIC3 are also calculated, as detailed in Appendix A. The good agreement between the simulated results and CMT provides additional validation for the proposed

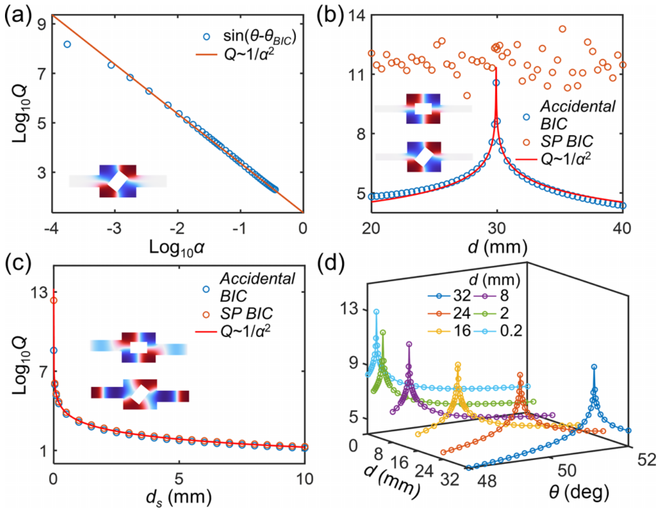

FIG. 3. (a) Dependence of the Q factor on the asymmetry parameter $\alpha = \sin(\theta - \theta_{\mathrm{BIC}})$. (b) Q factors of M_{22} versus d for SP BIC and accidental BIC. (c) Q factors of M_{22} versus d_s for SP BIC and accidental BIC. (d) Evolution of the Q factors distribution with respect to angle θ versus width d. Here, d is set as 32 mm, 24 mm, 16 mm, 8 mm, 2 mm, 0.2 mm, respectively. Insets show the eigenmode patterns.

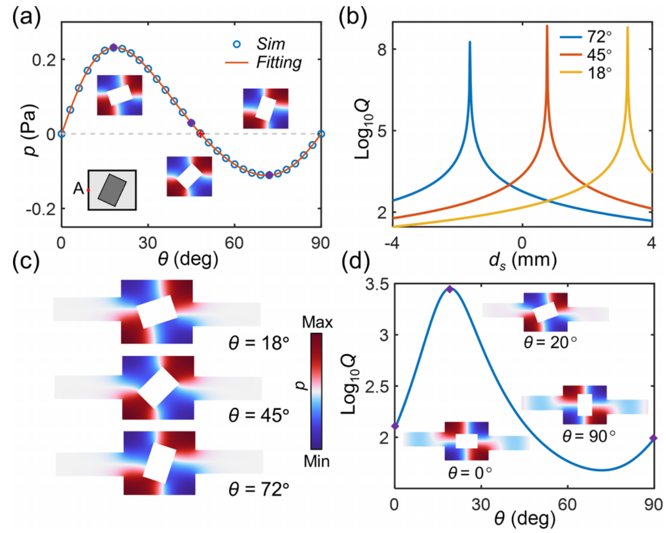

FIG. 4. (a) Eigenmode acoustic pressure at symmetric point A versus θ within a closed resonator. The red cross is located at (48.21°, 0 mm). (b) Q factors of M_{22} versus d_s with $\theta = 18°, 45°$, and $72°$, respectively. (c) Eigenmode patterns of accidental BICs at each angle. (d) Q factors of M_{22} versus θ with $d_s = 5$ mm. Insets show the eigenmode patterns.

model's utility in constructing BICs. Finally, we also presented the time-domain propagation of the QBIC in contrast with the low-Q mode, as illustrated in Fig. S1 [55]. For the QBIC angles, with a modulated Gaussian pulse incident, the QBIC is excited and sustained over an extended period due to its high-Q characteristic. Conversely, for the low-Q resonance, the acoustic wave gradually decays to nearly zero over time [55].

To deepen our understanding of the accidental BIC here, we investigate the interrelation between geometric parameters such as rotation angle θ, width d in the formation of BICs, and here we select BIC1 as demonstration. First, we analyze the variations of the Q factor of accidental BIC concerning asymmetry parameters $\alpha = \sin(\theta - \theta_{\mathrm{BIC}})$. Subsequently, an inverse quadratic correlation is discerned, as depicted in Fig. 3(a), demonstrating adherence to prior work [29]. Next, we undertake the analysis of width d. Here, we assume that $\theta = \theta_{\mathrm{BIC}}$ for both SP BIC and accidental BIC, then adjust the value of d. We find that the Q factor dramatically decreases for accidental BIC, while preserve relative high for SP BIC, as shown in Fig. 3(b). It should be noted that the variation of Q factors is mainly caused by numerical precision instead of the parameter adjustment. This phenomenon further demonstrates the existence of accidental BIC. In Fig. 3(c), we calculate the variations of the Q factor of the SP and accidental BICs with respect to the asymmetry parameter, denoted as $\alpha = d_s/d$, and both of them exhibit an inverse quadratic relationship with α. The differential results observed between the two asymmetric parameters can be attributed to the symmetry breaking in the structure. Finally, we also study the evolution of accidental BIC angles with d, as presented in Fig. 3(d). Here, we calculate the Q factor with the variation of θ, at $d = 32$ mm, 24 mm, 16 mm, 8 mm, 2 mm, and 0.2 mm, respectively. In the results obtained, we observe that the parameter θ converges towards a distinct value as d approaches an exceedingly small magnitude. To precisely determine the value, we compute the eigenmode pattern of M_{22} as a function of the angle θ in a closed resonator. Subsequently, we extract the total acoustic pressure at the midpoint on the left boundary, designated as symmetry point A, as depicted in Fig. 4(a). It should be noted that the rotation process will relocate the mode pattern, thus changing the value of acoustic pressure at the symmetry point, as illustrated in the insets of the mode pattern. The mode patterns here can be replicated approximately through the engineering of modes M_{22} and M_{31} [45]. When the zero-pressure nodal line aligns with the symmetry point, which corresponds to the intersections between the pressure distribution line and gray dash line, three angles 0°, 90°, and the specific angle 48.12° can be identified, respectively. The SP BICs (0°and 90°) will be preserved when attaching waveguides, while the middle mode gives rise to accidental BIC where the angle is dependent on the parameter of the waveguide. And this phenomenon is distinct to the resonators without obstacles, where the accidental BIC is degenerate to SP BIC, as shown in Fig. 9.

The formation of accidental BIC, as discussed above, is attributed to rotation of the obstacle in the above discussion. However, when the rotation angle deviates from θ_{BIC}, adjusting the waveguide's position can be employed to reconstruct the accidental BIC [45]. In our study, we examined rotation angles of $\theta = 18°$, 45°, and 72°, corresponding to relative maximum and minimum deviations within the rotation range [indicated by the purple quadrilateral in Fig. 4(a)]. At these angles, without waveguide adjustment, the modes function as QBICs with low quality factors. Effective reconstruction of the accidental BICs is achieved by varying the waveguide's lateral position (d_s) from −4 mm to 4 mm, as shown in Fig. 4(b). The adjustments in d_s correlate with the findings

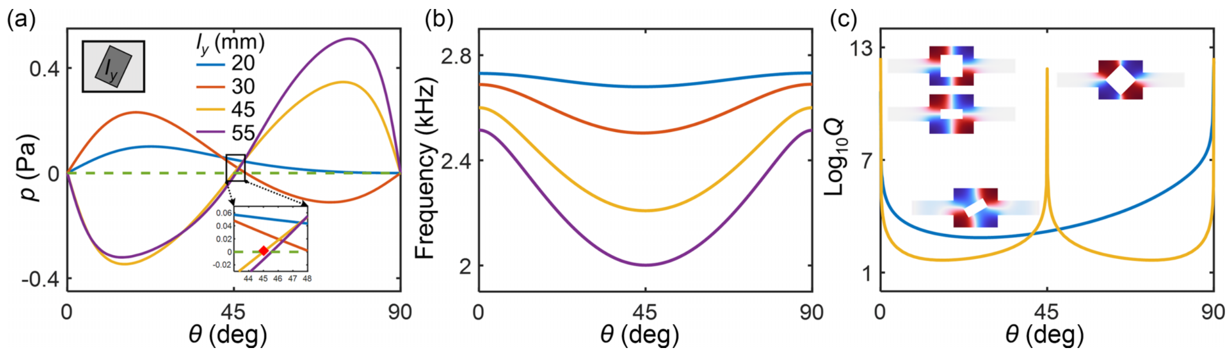

FIG. 5. (a) Eigenmode acoustic pressure at symmetric point A. (b) Eigenfrequency evolution versus θ with $l_y =$ 20 mm, 30 mm, 45 mm, 55 mm, respectively, within a closed resonator. (c) Q factors of M_{22} versus θ with $l_y = 20$ mm and 45 mm in a coupled-waveguide resonator system.

depicted in Fig. 4(a). For instance, at $\theta = 18^\circ$ the optimal d_s is a positive 3.24 mm, whereas at $\theta = 72^\circ$ it is a negative -1.62 mm, and at $\theta = 45^\circ$ it remains relatively minor at 0.76 mm. The eigenmode patterns, depicted in Fig. 4(c), further corroborate that the origins of accidental BICs stem from the modal symmetry with the waveguide. Additionally, our study also delineates the maximum effective range for d_s, beyond which, as demonstrated in Fig. 4(d), the entire range of rotation yields low-Q modes and fails to form BICs.

The investigation into mode pattern evolution reveals that specific rotation angles of BICs correlate with the geometric parameters of obstacles. Additionally, we have calculated the total acoustic pressure at the symmetry point across various obstacle widths, as shown in Fig. 5(a). Notably, a critical width ($l_y = 20$ mm) delineates a transition where zero-pressure nodal lines no longer align with symmetric points, indicating the annihilation of accidental BIC. As l_y increases, intersections between the 45° and 90° dashed lines become evident. Remarkably, when the obstacles are square ($l_x = l_y = 45$ mm), the pressure distribution remains symmetrical with respect to the rotation angle θ, as depicted by the yellow line in Fig. 5(a). At this configuration, an accidental BIC manifests at $\theta = 45^\circ$, marked by a red quadrilateral in the inset of Fig. 5(a). Thereafter, the formation angle of BIC will slightly deviate from 45° with an approaching value. Our findings further reveal that rectangular obstacle shapes contribute to an asymmetrical pressure distribution as the angle varies.

Further analysis of the eigenfrequency variations with θ in a closed resonator for the M_{22} mode is presented in Fig. 5(b). The extent of eigenfrequency variation increases with l_y, aligning with the trends observed in Fig. 5(a) and suggesting an evolution in mode shape. Additionally, we examine two specific cases ($l_y = 20$ mm and $l_y = 45$ mm) to calculate the variations in Q factors with θ when a waveguide is attached for demonstration. For $l_y = 20$ mm, the Q factors remain relatively low, with the exception of near 0° and 90°, suggesting the absence of accidental BICs. Conversely, for $l_y = 45$ mm, accidental BIC (also referred to as SP BICs) occur at $\theta = 45^\circ$, aligning well with observations from the closed resonators. The results we obtained highlights the impact of obstacle geometry within the system, underscoring the critical role of obstacle dimensions in the formation and evolution of BICs. The 2D model discussed above can be readily extended to a three-dimensional (3D) model for practical applications, as shown in Fig. S2 [55]. Further details on this extension are provided in the Supplemental Material [55].

III. MERGING BICS WITHIN SINGLE RESONATOR IN GEOMETRY SPACE

Acoustic resonators facilitate the engineering of various BICs, such as merging of FP BICs within pairs of resonators or a mirrored resonator [44]. In our study, by embedding rotational obstacles, we show the merging accidental BICs phenomenon in single resonator. As indicated in Fig. 2(a), we identify two accidental BICs, BIC2 and BIC3, within mode M_{32}. Subsequently, we explore the merging of these two BICs through modifications in the geometric configuration, as depicted in Fig. 6(a). Here, BIC2 and BIC3, characterized by rotation angles θ_2 and θ_3 respectively, converge into a single BIC at θ_m by adjusting the resonator length.

We initially analyzed the variation in the Q factor as a function of the angle θ while reducing the resonator length, as illustrated in Fig. 6(b). Decreasing the resonator length causes the two accidental BICs to approach each other in the angular space, represented by the orange and yellow lines in Fig. 6(b). Notably, these BICs merge into a single BIC when the length reduction reaches $\Delta L = -10.2$ mm, as indicated by the blue line in Fig. 6(b). The resultant merged BIC's angle is positioned between those of the original BICs. As the length decreases further to $\Delta L = -16$ mm, the merged BIC transitions into a QBIC, with relatively low Q factors across the entire rotation range, as shown by the brown curve in Fig. 6(b). Additionally, we also calculated the evolution of M_{32} within closed resonators, as depicted in Fig. S3 [55]. Prior to merging, two intersections between 0 and 90 degrees were observed, indicating the presence of two BICs. Conversely, in the merged case, only one intersection with the zero pressure line was found, indicating the presence of a single BIC.

We also present the Q-factor dependence on the asymmetry parameter $\alpha = \sin(\theta - \theta_{\mathrm{BIC}})$ with $\Delta L = -5$ mm and -10.2 mm, as shown in Fig. 6(c). At $\Delta L = -5$ mm, the calculated Q factors for BICs before merging exhibit an inverse quadratic correlation with the asymmetry parameter, illustrated by the yellow circles and purple curve in Fig. 6(c). Conversely, for the merged BIC ($\Delta L = -10.2$ mm), the calculated Q factors display an inverse quartic correlation

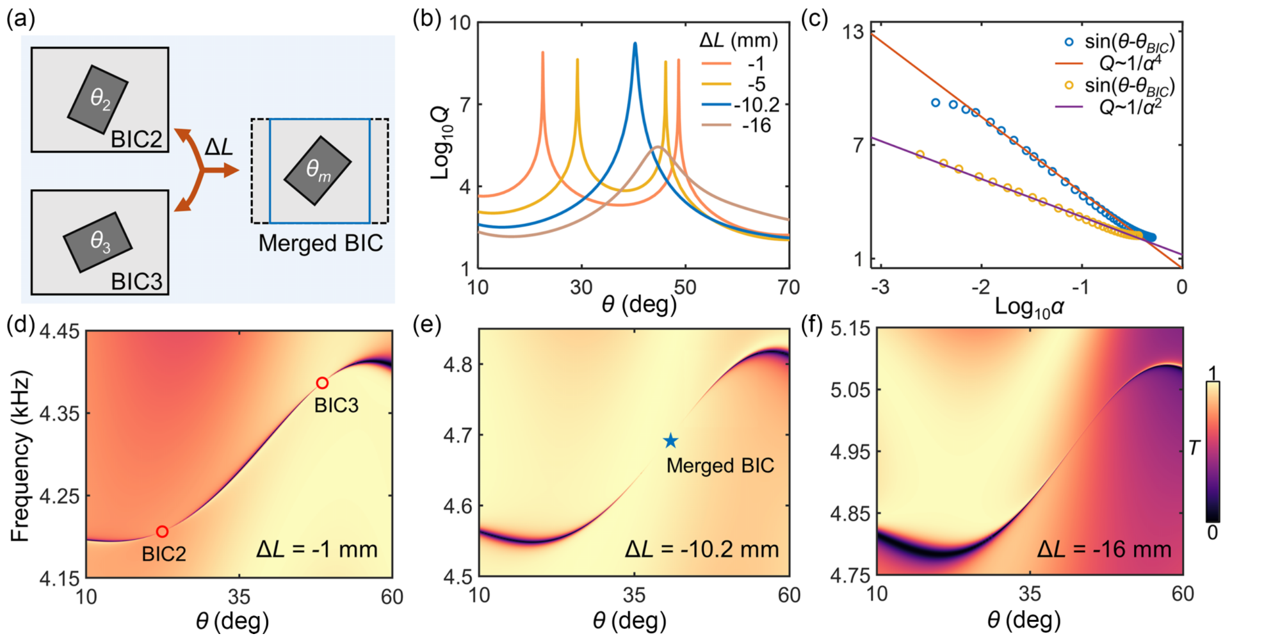

FIG. 6. Merging BICs in single resonator. (a) Schematic of the merging BICs utilizing geometry parameter. (b) Evolution of Q factors distribution versus angle θ. Here, ΔL is set as -1 mm, -5 mm, -10.2 mm, and -16 mm, respectively. (c) Dependence of the Q factor on the asymmetry parameter $\alpha = \sin(\theta - \theta_{\mathrm{BIC}})$ with $\Delta L = -5$ mm (before merge) and $\Delta L = -10.2$ mm (merged) (log-log scale). (d) Transmission spectrum of the single resonator around BIC2 and BIC3 (marked as red circles) before merging (e) for merged BIC (marked as blue star) and (f) after BIC merging.

with the asymmetry parameter, further demonstrating the merging phenomena, as depicted in blue circles and orange curve in Fig. 6(c). The slight discrepancies between the calculated results and the fitting curve may be attributed to numerical precision and proximity to another SP BIC near 0°. Typically, individual BICs may experience reduced Q factors due to scattering losses, which are caused by inevitable deviations during fabrication. Merging multiple BICs within geometric configurations offers a novel approach for enhancing Q factors in practical applications [44,56–59].

Additionally, we calculate the transmission spectrum for the cases of the BICs before merging, during merging, and after merging, as depicted in Figs. 6(d)–6(f). Initially, with $\Delta L = -1$ mm, two positions exhibiting zero linewidth are identified [marked with red circles in Fig. 6(d)], representing the individual BICs in the angular space before merging. Subsequently, reducing ΔL to the critical value of -10.2 mm resulted in a single zero-linewidth position [marked with a blue star in Fig. 6(e)], indicating the merger of the two BICs into a singular state. Further decreasing ΔL to -16 mm led to the continuation of mode M_{32} in the transmission spectrum, as shown in Fig. 6(f), illustrating the annihilation of the BIC. Moreover, the linewidth shown in Fig. 6(f) is broader compared with the previous cases, reflecting the relatively lower Q factors.

The merging BIC in geometry space can also be understood from the topological perspective. In periodical system like photonic crystals, the topological origin of the BIC is polarization singularity carrying topological charge in momentum space, contributing to their robustness [27]. However, in finite systems such as acoustic resonators where momentum space cannot be defined, BICs are characterized by topological charges of $q = +1$ and $q = -1$, indicated by phase singularities [44,60]. To generate phase singularities within our transmission system, it is necessary to shift the dispersion curve to the negative imaginary frequency axis. This alignment induces topological charges at the intersections of the dispersion curve and θ axis, manifesting as phase vortices. To address this, we introduced a slight artificial gain into the resonators, implemented by setting the sound velocity in the resonators to $v = 343 \times (1 - 2.5 \times 10^{-5} i)$ in our simulations.

We first calculate the eigenfrequency variation with respect to θ in the vicinity of BIC2, as shown in Fig. 7(a). For the lossless scenario, BIC2 is positioned at the zero of the eigenfrequency's imaginary component, indicating no coupling with the waveguide. In systems with induced gain, however, the eigenfrequency curve intersects the zero line at two points, corresponding to the topological charges near BIC2. Subsequently, we delineate two closed paths, C1 and C2, that encompass these intersections on the angle-frequency plane. The phase distributions along these paths are calculated and presented in Figs. 7(b) and 7(c). The topological charge is determined by the counter-clockwise phase accumulation around C1 and C2 as follows:

$$q = \frac{1}{2\pi} \oint d\phi. \tag{1}$$

Based on the equations presented, the topological charges of C1 and C2 can be determined as $q_1 = +1$ and $q_2 = -1$, respectively. The reflected phase exhibits analogous results, as illustrated in Fig. S4 [55]. Similarly, the topological charges for BIC3 and the merged BIC can be evaluated through the phase accumulation along closed paths depicted in Figs. 7(d)–7(i). These topological charges are $q_3 = +1$, $q_4 = -1$, $q_5 = +1$, and $q_6 = -1$. The concept of merging BICs from a topological perspective involves the cancellation of positive

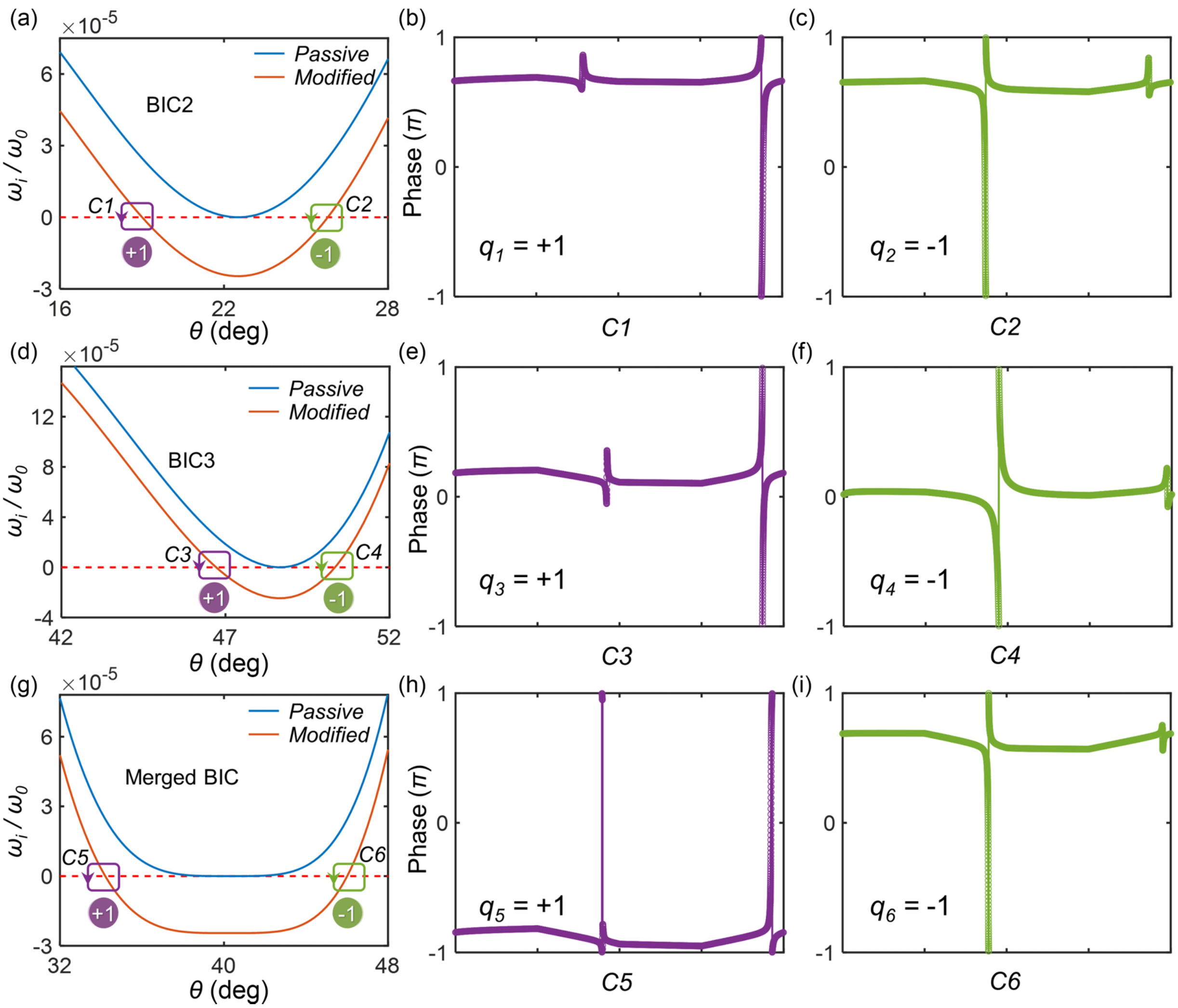

FIG. 7. Topological perspective of merging BICs. (a) Evolution of the imaginary part of the eigenfrequecy versus θ for BIC 2, (d) BIC 3, and (g) merged BIC. The blue curves represent the passive system and the orange curves represent the modified system, where a slight gain is introduced. (b), (c), (e), (f), (h), and (i) represent the phase distributions of closed paths C1 to C6 in the modified system, respectively, as marked in (a), (d), and (g).

and negative charges via superposition. In this study, as BIC2 and BIC3 converge closely on the angular frequency plane, their respective charges, $q_2 = -1$ and $q_3 = +1$, neutralize to zero, resulting in a merged BIC. To further elucidate this process, we have included a schematic diagram in Fig. S5 [55]. The proximity of these topological charges also indicates the robustness of the BIC; thus, the merged BIC exhibits increased robustness against external perturbations. Ultimately, the annihilation of BIC results from the neutralization of the existing topological charges.

IV. CONCLUSIONS AND DISCUSSION

In this work, we demonstrate the existence of accidental BICs in acoustic resonators embedded with rotating obstacles. These accidental BICs primarily depend on the mode symmetry at the interfaces between the waveguides and the resonator, effective only for modes that exhibit even distributions in the perpendicular propagation direction. This phenomenon is determined by changes in the coupling between the waveguides and the resonator, which vary with the rotational state of the embedded obstacle. Furthermore, these accidental BICs can be adjusted by modifying the waveguides and the obstacles' geometry parameters. By shifting the position or adjusting the dimensions of the attached waveguides, the QBICs can be translated into BICs, and vice versa. With the increased size of obstacles, the emergence and convergence of accidental BICs can be observed.

We also provide an effective method to identify the angles for BIC formation in closed resonators, further validated by resonators with attached waveguides. Additionally, we explore the dynamics of multiple accidental BICs within the M_{32} structure by varying the resonator's length, a model distinct from previous paired or mirrored-structure configurations that expands the potential for engineering BICs within the geometric parameter space of single resonator. We demonstrate that the Q factors of BICs before merging are inversely proportional to the square of the asymmetry parameters $\sin(\Delta\theta)$, Δd, and d_s, and a more robust inversely quartic relationship is observed for merged BIC, indicating enhanced high-Q stability against perturbations. The proposed 2D models can be projected into 3D models for practical application.

Our work provides an effective approach to identifying and manipulating the BICs within acoustic resonators, which may facilitate the selective excitation of QBICs and other control strategies. The principles established here are adaptable to resonators of various shapes, including cylindrical and spherical forms, and are effective with different obstacle shapes. Increasing the number of accidental BICs may require the utilization of higher-order modes, which warrants further investigation. This study aspires to guide the application of the findings in specialized scenarios, particularly within the domains of acoustic sensing and filtering.

ACKNOWLEDGMENTS

This work was supported by National Key Research and Development Program of China (Grants No. 2023YFA1407100 and No. 2020YFA0710100), Strategic Special Project of Guangdong Province (Grant No. GDZX2304005), Shenzhen Science and Technology Program (Grant No. JCYJ20210324121610028) and China Scholarship Council (Grant No. 202106310002).

APPENDIX A: COUPLED-MODE THEORY FOR TWO PORTS ACOUSTIC RESONATOR

The coupled-mode theory of the transmission or reflection coefficient of the two ports system we consider here can be written as follows [43,52]:

$$T(R) = \frac{(\omega-\omega_0)^2\cos^2\phi+\gamma^2\sin^2\phi\pm 2\sin\phi\cos\phi(\omega-\omega_0)\gamma}{(\omega-\omega_0)^2+\gamma^2}. \tag{A1}$$

Here, ω_0 is the resonance frequency, γ is the decay rate, and ϕ is the phase angle of the eigenfrequency. Both the real and imaginary parts of the complex eigenfrequencies are first calculated. By inserting the complex eigenfrequencies into Eq. (A1) and fitting the phase angle, the transmission coefficients can be predicted, and then compared with the simulation results.

In our study, the complex eigenfrequencies of QBIC1–3 are given as $\omega_1 = 2\pi\times(2625.47-0.021i)$ Hz, $\omega_2 = 2\pi\times(4173.96-0.035i)$ Hz, and $\omega_3 = 2\pi\times(4344.9-0.042i)$ Hz, respectively. The corresponding fitting parameters ϕ are 0.28π, 0.11π, and 0.054π. The transmission spectra for QBIC2 and QBIC3, as obtained from simulations and CMT, are presented in Figs. 8(a) and 8(b), respectively. The simulation results are consistent with CMT across all three cases.

APPENDIX B: MODE DECOMPOSITION IN THE RECTANGULAR RESONATOR

The eigenmodes of a closed rectangular resonator with Neumann boundary conditions can be written as

$$\psi_{mn}(x,y) = C_{mn}\cos\left[\frac{\pi(m-1)x}{L_x}\right]\cos\left[\frac{\pi(n-1)y}{L_y}\right],$$

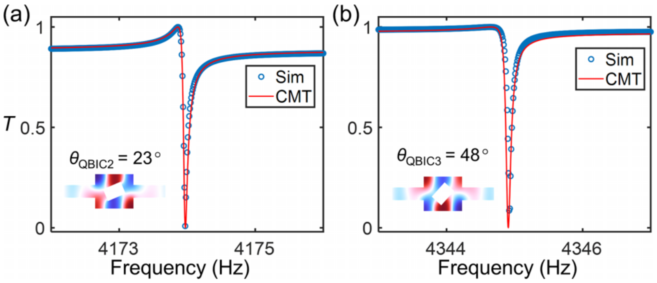

FIG. 8. The transmission spectrum of (a) QBIC2 with $\theta = 23^\circ$ and (b) QBIC3 with $\theta = 48^\circ$ using CMT and simulations. The inset shows patterns of QBICs.

$$\times\ (m, n = 1, 2, 3\ldots), \tag{B1}$$

where

$$C_{mn}^2 = \frac{(2-\delta_{m,1})(2-\delta_{n,1})}{L_xL_y} \tag{B2}$$

and L_x, L_y are the dimensions of the resonator.

As illustrated in Fig. 9(a), the accidental BIC discussed in the main text exhibits mode patterns similar to the FW BIC in rectangular resonators, which can be expressed as a superposition of the two eigenmodes (M_{22} and M_{31}) of the closed resonator by the following [45]:

$$\psi_{\rm BIC}(x,y) \approx g_1\psi_{22} + g_2\psi_{31}. \tag{B3}$$

Here, ψ_{22} and ψ_{31} are the eigenfunctions corresponding to the resonator modes M_{22} and M_{31}, respectively. The coefficients g_1 and g_2 are defined as $g_1 = \cos(\theta)$ and $g_2 = \sin(\theta)$. By adjusting the value of θ, we can modulate the contribution of each fundamental mode to the eigenmode pattern.

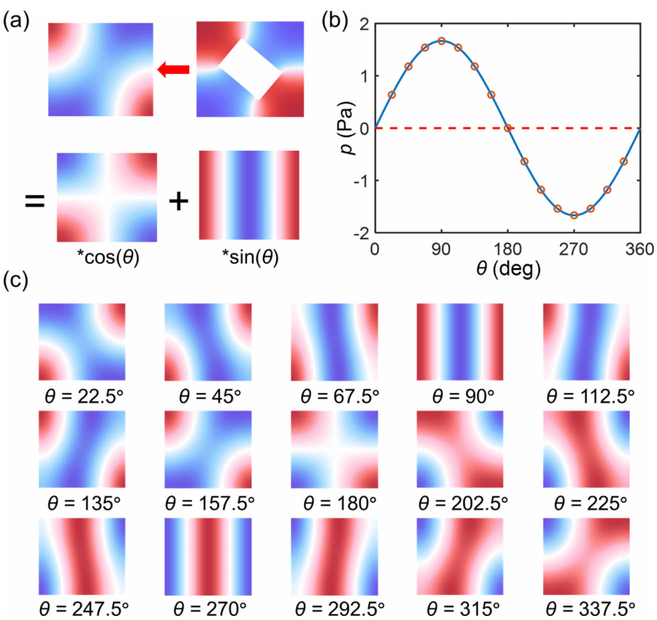

FIG. 9. Mode decomposition in a rectangular resonator without obstacle. (a) Schematic of the mode decomposition in rectangular resonator. (b) Acoustic pressure versus θ in the same point marked in Fig. 4(a). (c) mode pattern evolution at the orange circles marked in (b).

Further, we calculate the pressure for this superposed mode as θ varies, observed at the symmetry point referenced in the main text, depicted in Fig. 9(b). Unlike configurations with obstacles, variations in θ over a period of 2π do not lead to the formation of an accidental BIC. It should be noted that the intersection depicted in Fig. 9(b) locates at $\theta = 180^{\circ}$, where a SP BIC formed there. Additionally, the mode patterns highlighted by the orange circles in Fig. 9(a) underscore that in this instance, accidental BIC formation solely results from waveguide adjustments [45]. The introduction of a rotated obstacle in the resonators significantly enhances the flexibility of constructing BICs in acoustic resonators.

[1] A. E. Miroshnichenko, S. Flach, and Y. S. Kivshar, Fano resonances in nanoscale structures, Rev. Mod. Phys. **82**, 2257 (2010).

[2] F. Yesilkoy, E. R. Arvelo, Y. Jahani, M. Liu, A. Tittl, V. Cevher, Y. Kivshar, and H. Altug, Ultrasensitive hyperspectral imaging and biodetection enabled by dielectric metasurfaces, Nat. Photon. **13**, 390 (2019).

[3] A. Kodigala, T. Lepetit, Q. Gu, B. Bahari, Y. Fainman, and B. Kanté, Lasing action from photonic bound states in continuum, Nature (London) **541**, 196 (2017).

[4] Q. Ba, Y. Zhou, J. Li, W. Xiao, L. Ye, Y. Liu, J.-h. Chen, and H. Chen, Conformal optical black hole for cavity, eLight **2**, 19 (2022).

[5] Z. Feng, T. Shi, G. Geng, J. Li, Z.-L. Deng, Y. Kivshar, and X. Li, Dual-band polarized upconversion photoluminescence enhanced by resonant dielectric metasurfaces, eLight **3**, 21 (2023).

[6] C. W. Hsu, B. Zhen, A. D. Stone, J. D. Joannopoulos, and M. Soljačić, Bound states in the continuum, Nat. Rev. Mater. **1**, 16048 (2016).

[7] A. F. Sadreev, Interference traps waves in an open system: bound states in the continuum, Rep. Prog. Phys. **84**, 055901 (2021).

[8] J. von Neumann and E. P. Wigner, Über merkwürdige diskrete eigenwerte, Phys. Z. **30**, 467 (1929).

[9] F. Ursell, Trapping modes in the theory of surface waves, Math. Proc. Cambridge Philos. Soc. **47**, 347 (1951).

[10] R. Parker, Resonance effects in wake shedding from parallel plates: some experimental observations, J. Sound Vib. **4**, 62 (1966).

[11] R. Parker, Resonance effects in wake shedding from parallel plates: calculation of resonant frequencies, J. Sound Vib. **5**, 330 (1967).

[12] D. Evans and C. Linton, Trapped modes in open channels, J. Fluid Mech. **225**, 153 (1991).

[13] D. Evans, M. Levitin, and D. Vassiliev, Existence theorems for trapped modes, J. Fluid Mech. **261**, 21 (1994).

[14] E. Davies and L. Parnovski, Trapped modes in acoustic waveguides, Q. J. Mech. Appl. Math. **51**, 477 (1998).

[15] C. Linton, M. McIver, P. McIver, K. Ratcliffe, and J. Zhang, Trapped modes for off-centre structures in guides, Wave Motion **36**, 67 (2002).

[16] Y. Duan, W. Koch, C. M. Linton, and M. McIVER, Complex resonances and trapped modes in ducted domains, J. Fluid Mech. **571**, 119 (2007).

[17] C. Linton and P. McIver, Embedded trapped modes in water waves and acoustics, Wave Motion **45**, 16 (2007).

[18] S. Hein and W. Koch, Acoustic resonances and trapped modes in pipes and tunnels, J. Fluid Mech. **605**, 401 (2008).

[19] S. Hein, W. Koch, and L. Nannen, Fano resonances in acoustics, J. Fluid Mech. **664**, 238 (2010).

[20] P. McIver and M. McIver, Motion trapping structures in the three-dimensional water-wave problem, J. Eng. Math. **58**, 67 (2007).

[21] P. Cobelli, V. Pagneux, A. Maurel, and P. Petitjeans, Experimental observation of trapped modes in a water wave channel, Europhys. Lett. **88**, 20006 (2009).

[22] C. Fitzgerald and P. McIver, Passive trapped modes in the water-wave problem for a floating structure, J. Fluid Mech. **657**, 456 (2010).

[23] P. Cobelli, V. Pagneux, A. Maurel, and P. Petitjeans, Experimental study on water-wave trapped modes, J. Fluid Mech. **666**, 445 (2011).

[24] D. C. Marinica, A. G. Borisov, and S. V. Shabanov, Bound states in the continuum in photonics, Phys. Rev. Lett. **100**, 183902 (2008).

[25] Y. Plotnik, O. Peleg, F. Dreisow, M. Heinrich, S. Nolte, A. Szameit, and M. Segev, Experimental observation of optical bound states in the continuum, Phys. Rev. Lett. **107**, 183901 (2011).

[26] C. W. Hsu, B. Zhen, J. Lee, S.-L. Chua, S. G. Johnson, J. D. Joannopoulos, and M. Soljačić, Observation of trapped light within the radiation continuum, Nature (London) **499**, 188 (2013).

[27] B. Zhen, C. W. Hsu, L. Lu, A. D. Stone, and M. Soljačić, Topological nature of optical bound states in the continuum, Phys. Rev. Lett. **113**, 257401 (2014).

[28] M. V. Rybin, K. L. Koshelev, Z. F. Sadrieva, K. B. Samusev, A. A. Bogdanov, M. F. Limonov, and Y. S. Kivshar, High-Q supercavity modes in subwavelength dielectric resonators, Phys. Rev. Lett. **119**, 243901 (2017).

[29] K. Koshelev, S. Lepeshov, M. Liu, A. Bogdanov, and Y. Kivshar, Asymmetric metasurfaces with high-Q resonances governed by bound states in the continuum, Phys. Rev. Lett. **121**, 193903 (2018).

[30] J. Lee, B. Zhen, S.-L. Chua, W. Qiu, J. D. Joannopoulos, M. Soljačić, and O. Shapira, Observation and differentiation of unique high-Q optical resonances near zero wave vector in macroscopic photonic crystal slabs, Phys. Rev. Lett. **109**, 067401 (2012).

[31] H. Friedrich and D. Wintgen, Interfering resonances and bound states in the continuum, Phys. Rev. A **32**, 3231 (1985).

[32] A. F. Sadreev, E. N. Bulgakov, and I. Rotter, Bound states in the continuum in open quantum billiards with a variable shape, Phys. Rev. B **73**, 235342 (2006).

[33] E. N. Bulgakov and A. F. Sadreev, Bound states in the continuum in photonic waveguides inspired by defects, Phys. Rev. B **78**, 075105 (2008).

[34] S. Weimann, Y. Xu, R. Keil, A. E. Miroshnichenko, A. Tünnermann, S. Nolte, A. A. Sukhorukov, A. Szameit, and Y. S. Kivshar, Compact surface fano states embedded in the

continuum of waveguide arrays, Phys. Rev. Lett. **111**, 240403 (2013).

[35] E. Bulgakov, A. Pilipchuk, and A. Sadreev, Desktop laboratory of bound states in the continuum in metallic waveguide with dielectric cavities, Phys. Rev. B **106**, 075304 (2022).

[36] A. S. Pilipchuk and A. Sadreev, Accidental bound states in the continuum in an open Sinai billiard, Phys. Lett. A **381**, 720 (2017).

[37] S. Hein, W. Koch, and L. Nannen, Trapped modes and Fano resonances in two-dimensional acoustical duct–cavity systems, J. Fluid Mech. **692**, 257 (2012).

[38] A. Lyapina, D. Maksimov, A. Pilipchuk, and A. Sadreev, Bound states in the continuum in open acoustic resonators, J. Fluid Mech. **780**, 370 (2015).

[39] A. Lyapina, A. Pilipchuk, and A. Sadreev, Trapped modes in a non-axisymmetric cylindrical waveguide, J. Sound Vib. **421**, 48 (2018).

[40] A. Lyapina, A. Pilipchuk, and A. Sadreev, Bound states with orbital angular momentum in the continuum of cylindrical non-axisymmetric waveguide, Ann. Phys. **396**, 56 (2018).

[41] W. Li, J. Zou, K. Lee, and X. Li, Asymmetric trapped modes in a tube waveguide with a bulge, Acta Mech. **229**, 1123 (2018).

[42] S. Huang, T. Liu, Z. Zhou, X. Wang, J. Zhu, and Y. Li, Extreme sound confinement from quasibound states in the continuum, Phys. Rev. Appl. **14**, 021001(R) (2020).

[43] L. Huang, Y. K. Chiang, S. Huang, C. Shen, F. Deng, Y. Cheng, B. Jia, Y. Li, D. A. Powell, and A. E. Miroshnichenko, Sound trapping in an open resonator, Nat. Commun. **12**, 4819 (2021).

[44] L. Huang, B. Jia, Y. K. Chiang, S. Huang, C. Shen, F. Deng, T. Yang, D. A. Powell, Y. Li, and A. E. Miroshnichenko, Topological supercavity resonances in the finite system, Adv. Sci. **9**, 2200257 (2022).

[45] L. Huang, B. Jia, A. S. Pilipchuk, Y. Chiang, S. Huang, J. Li, C. Shen, E. N. Bulgakov, F. Deng, D. A. Powell, S. A. Cummer, Y. Li, A. F. Sadreev, and A. E. Miroshnichenko, General framework of bound states in the continuum in an open acoustic resonator, Phys. Rev. Appl. **18**, 054021 (2022).

[46] A. Sadreev, E. Bulgakov, A. Pilipchuk, A. Miroshnichenko, and L. Huang, Degenerate bound states in the continuum in square and triangular open acoustic resonators, Phys. Rev. B **106**, 085404 (2022).

[47] I. Deriy, I. Toftul, M. Petrov, and A. Bogdanov, Bound states in the continuum in compact acoustic resonators, Phys. Rev. Lett. **128**, 084301 (2022).

[48] B. Jia, L. Huang, A. S. Pilipchuk, S. Huang, C. Shen, A. F. Sadreev, Y. Li, and A. E. Miroshnichenko, Bound states in the continuum protected by reduced symmetry of three-dimensional open acoustic resonators, Phys. Rev. Appl. **19**, 054001 (2023).

[49] Z. Zhou, B. Jia, N. Wang, X. Wang, and Y. Li, Observation of perfectly-chiral exceptional point via bound state in the continuum, Phys. Rev. Lett. **130**, 116101 (2023).

[50] H. Zhang, S. Liu, Z. Guo, S. Hu, Y. Chen, Y. Li, Y. Li, and H. Chen, Topological bound state in the continuum induced unidirectional acoustic perfect absorption, Sci. China Phys. Mech. Astron. **66**, 284311 (2023).

[51] D. N. Maksimov, A. F. Sadreev, A. A. Lyapina, and A. S. Pilipchuk, Coupled mode theory for acoustic resonators, Wave Motion **56**, 52 (2015).

[52] S. Fan, W. Suh, and J. D. Joannopoulos, Temporal coupled-mode theory for the Fano resonance in optical resonators, J. Opt. Soc. Am. A **20**, 569 (2003).

[53] L. Cao, Y. Zhu, S. Wan, Y. Zeng, Y. Li, and B. Assouar, Perfect absorption of flexural waves induced by bound state in the continuum, Extreme Mech. Lett. **47**, 101364 (2021).

[54] O. Gbidi and C. Shen, Selectively exciting quasibound states in the continuum in open microwave resonators using dielectric scatters, Phys. Rev. B **107**, 184309 (2023).

[55] See Supplemental Material at http://link.aps.org/supplemental/10.1103/PhysRevB.110.054201 for detail of time-domain propagation of acoustic waves in resonators with rotating obstacles, the extension of planar design to 3D realization, eigenmode acoustic pressure for high-order mode inside closed resonators, reflected phase distributions, and schematic of the evolution of topological charges during merging process

[56] J. Jin, X. Yin, L. Ni, M. Soljačić, B. Zhen, and C. Peng, Topologically enabled ultrahigh-Q guided resonances robust to out-of-plane scattering, Nature (London) **574**, 501 (2019).

[57] M. Kang, S. Zhang, M. Xiao, and H. Xu, Merging bound states in the continuum at off-high symmetry points, Phys. Rev. Lett. **126**, 117402 (2021).

[58] M. Kang, L. Mao, S. Zhang, M. Xiao, H. Xu, and C. T. Chan, Merging bound states in the continuum by harnessing higher-order topological charges, Light Sci. Appl. **11**, 228 (2022).

[59] S. Yu, Z. Li, R. Chai, W. Liu, W. Zhou, H. Cheng, and S. Chen, Merging bound states in the continuum in the geometrical parameter space, Phys. Rev. B **109**, 115109 (2024).

[60] Z. Sakotic, A. Krasnok, A. Alú, and N. Jankovic, Topological scattering singularities and embedded eigenstates for polarization control and sensing applications, Photon. Res. **9**, 1310 (2021).